Gen Shibata, Kensei Karumai, Suzune Sakai, and Hideyuki Ogawa

Title: Study on partial oxidation phenomena of post-injection fuel in diesel engines

Abstract

In diesel engines, post fuel is injected in the expansion stroke, oxidized by the diesel oxidation catalysts and the high temperature gas re-generates the diesel particulate filters. However, it is empirically known that the post fuel at advanced injection timing is partially oxidized in the cylinder due to the high temperature-pressure conditions and it is a cause of the reduction of fuel consumption.

The purpose of this research is to analyze post-injection fuel behaviors in cylinder and investigate the optimum fuel injections that maximize the unburnt hydrocarbons to the diesel oxidation catalysts. The engine employed in this research is a turbo charged 2.0 litter four-cylinder DI diesel engine with two fuel injection systems to change the heterogeneity of air-fuel mixture and temperature distributions in cylinder; n-hexane is injected in the intake manifold to produce the homogeneous air-fuel mixture and diesel fuel is directly injected into the cylinder. The partial oxidation ratio of post fuel and the fuel loss mainly by fuel adhesion was calculated by injected fuel quantity, air quantity, and emission data. The 3D-CFD software was introduced to analyze the partial oxidation of post fuel and flow in the cylinder. The heterogeneity of burned gas mixture of post injection atmosphere and the post-injection timings were the parameters of engine tests and 3D-CFD simulations.

The results suggest that the heterogeneity of equivalence ratio and the non-uniformity of gas temperature inside the cylinder at the start of post injection affect the partial oxidation of post-injection fuel. The more homogeneous these conditions are, the better the suppression of partial oxidation of post-injection fuel and the avoidance of fuel adhesion to the cylinder wall can be achieved.

Keywords: Diesel Engine, Post Fuel Injection, Partial Oxidation, In-cylinder Temperature, Equivalence Ratio, Heterogeneity

Nomenclature:

°CA ATDC	Crank angle after top dead center
DOC	Diesel oxidation catalyst
DPF	Diesel particulate filter
PM	Particulate matter
THC	Total hydrocarbon counted as methane

Greek symbols:

ϕ	Inner diameter of constant volume chamber or injector hole
θ_{post}	Post injection timing

Introduction

In diesel engines, post fuel is injected in the expansion stroke, oxidized by the diesel oxidation catalysts (DOC) and the generated high temperature gas re-generates the diesel particulate filters (DPF). Much post injection research has been conducted. Serrano investigated the dynamics of late fuel post-injection flow and the oxidation processes of hydrocarbons (HCs) in DOC, as well as the soot oxidation mechanism in DPF [1]. Yamamoto utilized Pt or Pt/Pd based DOC catalysts and examined HC emissions especially polycyclic aromatic hydrocarbons after the DOC oxidation [2]. Bobba operated the diesel engine under the low-temperature combustion conditions, and the generation of soot in piston bowl and squish area was analyzed using the high-speed two-color method to investigate the effects of post-injection timing on soot generation [3]. O'Connor explained the effects of post-injection on soot reduction in the DPF, and introduced the effects of engine operation parameters on DPF soot reduction [4]. Jeftic studied the effects of post-injection with diverse SOI on the formation of hydrogen and light HCs species [5] and reported that the early post-injection generates high temperature, producing lower CO, THC and light hydrocarbons due to stronger fuel oxidation of main injection. Additionally, if the fuel is combusted within the cylinder, it will result in work during the expansion stroke and cooling losses, thereby insufficiently supplying heat to the DPF. These results suggest that the oxidation or partial oxidation of post-injection fuel significantly reduces the amounts of generated hydrocarbons, thereby insufficiently supplying hydrocarbons to the DOC.

Martin operated the light-duty diesel engine with parameters of post-injection duration and the commanded dwell time between main and post injections, and investigated the post-injection strategies on the soot reduction [6]. Wu investigated the effects of post-injection timing and quantity on diesel exhaust emission [7].

Further, some research groups have investigated the post-fuel adhesion on the cylinder wall. Kojima constructed a zero-dimensional numerical calculation model to predict the amount of fuel adhering to the cylinder wall when post fuel is injected into the combustion chamber of diesel engine [8], [9]. Ito et al. investigated the effects of engine operating conditions and lubricants oil temperature on the evaporation of diesel fuel components mixed into the lubricants oil [10], [11], [12], [13] and they developed an empirical model coupled with Kojima's model to account for these effects. To reduce post fuel adhesion and oil splashing on the cylinder wall, it is necessary to advance the timing of post fuel injection. However, as previously reported by Budde and Pischinger [14], advanced post fuel injection may lead to partial oxidation of the post fuel. The oxidation and adhesion behaviors of post fuel are highly dependent on the in-cylinder conditions.

In our laboratory, an analysis of the wall impingement phenomena of post-injection fuel has been carried out using a visualized constant volume chamber. The temperature and pressure conditions inside the cylinder during post injection are formed within this chamber, and observations of spray evaporation under oxygen-free conditions using Mie scattering and Schlieren methods [15] have been conducted, as well as the quantity of splashed oil by post fuel impingement was also investigated [16]. In early post injection, the fuel evaporates before impacting the cylinder wall. However, by delaying the post-injection timing, the ambient temperature and pressure decrease, causing the liquid phase within the spray to gradually extend and collide with the cylinder wall, resulting in the splashing of the oil film on the cylinder wall. It was also observed that post fuel, after the impingement of the cylinder wall, flows along the wall into the piston and cylinder crevice, and is absorbed into the engine oil on the cylinder wall.

As observation in the constant volume chamber only allows for spray analysis, quantification was also performed through engine experiments. Carbon balance and oxygen balance were calculated based on the fuel supplied to the engine and exhaust gas concentrations, enabling the quantification of the amount of post-injection fuel diluted in the engine oil due to combustion and wall impingement [17]. The results revealed that as the post fuel injection timing is retarded, the transition from partial oxidation to oil dilution during normal post injection is continuous. Additionally, these experiments suggest that partial oxidation during post injection is influenced by the non-uniformity distributions of equivalence ratios and temperature after the main diesel combustion.

In this paper, we focused the partial oxidation phenomena of post-injection fuel. Based on the findings, the dual-fuel engine was introduced to change the temperature non-uniformity and equivalence ratio heterogeneity in the cylinder. The goal is to make clear the impact of non-uniformity distributions of equivalence ratios and temperature in the cylinder on subsequent partial oxidation of post-injection fuel through engine experiments and 3D-CFD analysis.

Experimental methods

Engine setup

The layout of the test engine and measurement instruments is shown in Figure 1. The engine employed in the experiment is a research, turbo charged, 2.0L, 4-cylinder direct injection diesel engine with a compression ratio of 15.8. Figure 2 shows the shape of re-entrant piston top of this engine. The intake air flow rate was measured by a thermal mass flow meter installed upstream of the turbo charger compressor, and instantaneous recordings were performed using the automotive ECU calibration tool INCA. The exhaust emissions are analyzed using the emission analyzer Horiba MEXA-1600 and Best Sokki FTIR BOB 2000FT, and the total molar number of exhaust emissions is calculated. The specifications of the test engine are listed in Table 1. The test engine is equipped with a common rail injection system using JIS No.2 diesel fuel as the test fuel, and it also has a port fuel injector on the intake manifold to enable HCCI operation with n-hexane (n-C_6H_{14}), allowing for dual-fuel operation. The ignitability of diesel fuel and n-hexane are similar, and the combustion of premixing and direct injection is employed to investigate how the heterogeneity of equivalence ratio and the non-uniformity of gas temperature inside the cylinder affect the ignitability of post-injection fuel. It looks like an RCCI engine in terms of system, however the research purpose is not to conduct research on RCCI combustion.

The engine is equipped with an intake heater, a turbocharger, and an intake restrictor, allowing independent adjustment of intake air temperature and pressure. The details of the diesel fuel are shown in Table 2. The hydrocarbon composition of the JIS No. 2 diesel fuel was analyzed by a gas chromatograph time-of-flight mass spectrometer (GC TOF-MS) and the average molecular weight was 227.19 ($C_{16.36}H_{30.49}$). Figure 3 provides a schematic diagram of the constructed n-hexane injection system. The n-hexane is easily vaporized and used to form the well premixed gas charge with air in the intake manifold to achieve the HCCI combustion. A 360 °CA pulse signal is generated by optical angle detector directly connected to the crankshaft of the test engine and n-hexane, pressurized to approximately 350 kPa using a fuel pump, is injected from a port fuel injector installed on the intake manifold in the mainstream direction at the same timing in each cycle. The injection volume of n-hexane is controlled by adjusting the pulse width of the 5V pulse signal output using the pulse width adjustment dial provided on the pulse generator.

Calculations of fuel loss and oxidation ratio of the post-injection fuel

In the engine tests, the fuel loss, mainly due to oil dilution, and the oxidation of the post fuel were calculated from the exhaust emission data; oxygen, nitrogen oxide, unburned hydrocarbons (THC), carbon monoxide (CO), and carbon dioxide (CO_2), simultaneously measured by a Horiba MEXA-1600 DEGR and water vapor (H_2O) by a Best Sokki BOB-2000FT. The reaction equation for one cycle in the cylinder can be described as shown in equation 1. In the diesel engine emissions, the nitrogen oxide (NOx) in the exhaust manifold is mainly nitrogen monoxide (NO) and the NO is used in equation 1 as a NOx representative.

$$A\cdot fuel+B\cdot O_{2\_in}+C\cdot N_{2\_in}+D\cdot CO_{\_2in}+E\cdot H_2O_{\_in}+F\cdot CO_{\_in}+G\cdot THC_{\_in}+H\cdot NO_{\_in}$$
$$= a\cdot CO_{2\_ex}+b\cdot H_2O_{\_ex}+c\cdot N_{2\_ex}+d\cdot O_{2\_ex}+e\cdot CO_{\_ex}+f\cdot NO_{\_ex}+g\cdot THC_{\_ex}+n_{loss} \quad (1)$$

fuel: JIS No. 2 diesel fuel, the average structure is $C_{16}H_{32}$

in: Subscript that shows intake gas

ex: Subscript that shows exhaust gas

n_{loss}: Fuel loss mainly due to oil dilution

A-H and a-g: Coefficients in the reaction

Equations 2 and 3 show the conservation of mass for carbon or oxygen in the left and right members respectively in equation 1,

The conservation of carbon atoms:

$$16A + D + F + G = a + e + g + 16\ n_{loss} \tag{2}$$

The conservation of oxygen atoms:

$$2B + 2D + E + F + H = 2a + b + 2d + e + f \tag{3}$$

From the carbon balance in equation 2, the molecule number of the total gas in the exhaust (n_{ex}(C)) can be expressed as shown in equation 4.

$$n_{ex}(C) = \frac{16(n_{fuel} - n_{loss}) + n_{air+EGR}\left(X_{CO_2} + X_{THC} + X_{CO}\right)_{air+EGR}}{\left(X_{CO_2} + X_{THC} + X_{CO}\right)_{ex}} \tag{4}$$

In equation 4, X_{CO_2}, X_{THC}, and X_{CO} express the molar ratios in the total air or exhaust gas. For example, the molar ratios of carbon dioxide in the intake ($X_{CO_2,\ in}$) and exhaust ($X_{CO_2,\ ex}$) are calculated as $X_{CO_2,\ in}$=D/n_{in} and $X_{CO_2,\ ex}$=a/n_{ex} respectively, and n_{in} and n_{ex} show the total molar number of the working gas in the intake and exhaust.

Similarly, the molecule number of the total gas in the exhaust (n_{ex}(O)) can also be calculated from the oxygen balance in equation 3 as shown in equation 5.

$$n_{ex}(O) = \frac{n_{air+EGR}\left(2X_{O_2} + 2X_{CO_2} + X_{H_2O} + X_{NO} + X_{CO}\right)_{air+EGR}}{\left(2X_{O_2} + 2X_{CO_2} + X_{H_2O} + X_{NO} + X_{CO}\right)_{ex}} \tag{5}$$

Using the Solver function in the Excel software, the fuel loss (n_{loss}) can be optimized to let the calculation results of equations 4 and 5 be the same values (n_{ex}(C)=n_{ex}(O)).

Further, the oxidation ratio of the post fuel is calculated from the carbon balance of CO_2, CO, and THC emission data measured by the exhaust gas analyzer, as suggested in equation 6.

$$\eta_{oxidation\ ratio,post\ fuel} = 100 \cdot \frac{16n_{fuel,post} - \left(n_{ex}(X_{CO_2} + X_{CO} + X_{THC})_{ex} - 16n_{fuel,main} \cdot (1 - \eta_{comb,main})\right) - 16n_{loss}}{16n_{fuel,post}} \tag{6}$$

$\eta_{oxidation\ ratio,\ post\ fuel}$: Oxidation ratio of the post fuel [%]

$n_{fuel,main}$: Molar number of the main injection fuel

$n_{fuel,post}$: Molar number of the post-injection fuel

n_{ex}: Total molar number of the exhaust gas

$\eta_{comb,\ main}$: Combustion efficiency of the main combustion [%]

The accuracy of the fuel loss (η_{loss}) and oxidation ratio in the calculations were evaluated in the reference paper [17].

Three-dimensional CFD analysis

In this study, numerical analysis of ignition and combustion characteristics of post-injection fuel spray was conducted using three-dimensional computational fluid dynamics (3D-CFD) analysis software, AVL-FIRE ver. 2020.

The calculation focused on a test engine used in experiments, and its main parameters are shown in Table 1. The computational mesh of the re-entrant type combustion chamber at TDC is shown in Figure 4. Since the injector of the test engine is a 9-hole nozzle, a sector model was used to reduce computational load, dividing the combustion chamber into 1/9 in the circumferential direction. The average cell size is 0.5mm, and the wall-adjacent boundary cells have a thickness of 0.2 mm in a 4-layer structure, resulting in a total of 97600 cells. The compression ratio was adjusted by altering the squish height.

In Table 3, the sub-models used in this calculation are presented. The combustion spray is modeled using the discrete droplet model (DDM), and the initial droplet size of the spray is set to be equivalent to the injector nozzle diameter. For the primary and secondary breakup of the fuel spray, the Kelvin-Helmholtz and Rayleigh-Taylor model (KH-RT model) [18] is used, the Dukowicz model [19] is employed for the evaporation model, and the Han-Reitz model [20] is used for the heat transfer model. The model constants for each model were set as follows.

KH-RT model constants:
C1=0.61, C2=12, C3=10, C4=5.33, C5=1.0, C6=0.3, C7=0.05, C8=0.188

Dukowicz model constants:
E1=100, E2=1.0

Due to computational constraints, the ECFM-3Z model [21] was used as the combustion model and the computational domain was divided into three regions; a non-mixing region consisting of pure air and EGR, a mixing region of air and fuel, and a non-mixing region consisting of pure fuel. Further, each region is divided into two zones; unburned gas region and burned gas region, and self-ignition is calculated in the unburned gas region, premixed combustion is calculated at the boundary between the unburned gas and the burned gas regions, and diffusion combustion is calculated in the burned gas region.

The model constants for the ECFM-3Z model are adjusted based on the specific conditions under investigation. The κ–ζ–f turbulence model is employed [22], [23], and for the fuel, n-heptane, which has similar ignition characteristics to diesel fuel, is used.

The impact of homogeneity circumstances in cylinder on the partial oxidation of single stage post fuel injection (Engine experiments)

Three types of engine experiments from Test 1 to Test 3 were conducted. In all DPF regeneration conditions, the engine speed was 1200 rpm, and the IMEP ranged from 0.2-0.25MPa. The smoke generated under these conditions was 0 BSU (Bosch smoke unit), and the experiments were conducted under conditions that did not affect the deposition of soot on the DPF.

Partial oxidation behavior of post-injection fuel under conventional DPF re-generation operating conditions (Test 1)

Engine test conditions

To analyze the fundamental partial oxidation reactions of post-injection fuel, a single-stage post injection was employed, and the impact of in-cylinder air inhomogeneity during post injection on partial oxidation of single stage post fuel injection was investigated.

The conditions of experiment are presented in Table 4, and various conditions were investigated, including conditions where all of the post-injection fuel burns, conditions where partial oxidation occurs, and conditions where no further heat generation occurs. To achieve these conditions, the post-injection timing (θ_{post}) was varied in 11 steps within the range of 25 °CA ATDC to 60 °CA ATDC, and the total injection quantity for pilot, pre, and main injections was set at 12.0 mm^3/cycle, to maintain in-cylinder average oxygen concentration of 16.0% during post injection, while the post-injection quantity was maintained constant at 5.0mm^3/cycle.

Test results and discussions in Test 1

In Figure 5, the emissions concentrations of THC and CO at various post-injection timings (θ_{post}) are shown, and Figure 6 presents the heat release ratio of post-injection fuel. The heat release data of post-injection fuel are listed in Figure AP-1 in Appendix.

The average temperature history due to the combustion of pilot injection, pre-injection, and main injection is the same in each plot, however, the later the post-injection timing, the lower the temperature and pressure at the start of post-injection decreases as the piston descends. As the post-injection timing is retarded, the heat release ratio of post-injection fuel gradually decreases, and partial oxidation of post fuel injection is observed between 40-52.5 °CA ATDC. At post-injection timings earlier than 35 °CA ATDC, all the post-injection fuel is combusted and the CO emissions concentration is low, however at post-injection timings of 40-52.5 °CA ATDC, where partial oxidation is evident, the CO emissions concentration significantly increases, suggesting that CO is being emitted without undergoing oxidation to CO_2. As the post-injection timing is further retarded, the CO emissions concentration decreases, due to insufficient progress in the oxidation reactions of post-injection fuel, and as the percentage of heat release ratio decreases, the THC emissions concentration increases. Retarding the post-injection timing beyond 47.5 °CA ATDC can suppress the partial oxidation of post-injection fuel and enable the supply of mist-like diesel fuel to the DOC, however excessive post-injection retardation can lead to challenges related to lubricating oil dilution caused by cylinder wall impingement.

Partial oxidation behavior of post-injection fuel in air/fuel homogeneous mixture conditions (Test 2)

To focus on the partial oxidation phenomena of post-injection fuel, experiments were conducted by creating a high temperature and pressure homogeneous ambient atmosphere within the cylinder through HCCI combustion using n-hexane as the test fuel. The partial oxidation phenomena were evaluated during conditions where the ambient temperature and equivalence ratio at the start of post injection were homogenized.

Engine test conditions

The conditions of this experiment are presented in Table 5. The engine was operated in a homogeneous charge compression ignition (HCCI) mode with n-hexane premixed charge, and post-fuel injection was performed in a homogeneous atmosphere with uniform temperature and equivalence ratio distribution within the cylinder. Various conditions were investigated, including conditions where all of the post-injection fuel burns, conditions where partial oxidation occurs, and conditions where no further heat generation occurs. To achieve these conditions, the post-injection timing (θ_{post}) was varied in 8 steps within the range of 25-40 °CA ATDC, and the equivalence ratio of n-hexane was adjusted to maintain an in-cylinder average oxygen concentration of 16.0% during post injection, and two post-injection quantities of 2.5 mm^3/cycle and 5.0 mm^3/cycle were set.

Test results and discussions in Test 2

In Figure 7, the emission concentrations of THC and CO at various post-injection timings are shown and Figure 8 presents the heat release ratio of post-injection fuel. The heat release data of post-injection fuel are listed in Figure AP-2 in Appendix.

The average temperature history due to the HCCI combustion is the same in each plot, however, the later the post-injection timing, the lower the temperature and pressure at the start of post-injection decreases as the piston descends. While in Test 1 (Figure 6), partial oxidation of post-injection fuel was observed over the range of post-injection timing between 40 to 52.5 °CA ATDC, when single stage post injection was conducted into the high temperature and pressure homogeneous circumstance formed by HCCI combustion, partial oxidation only occurred within a narrow range of post-injection timing specifically between 32-34 °CA ATDC. This suggests that the partial oxidation reactions of post-injection fuel are significantly dependent on the heterogeneity of equivalence ratio and the non-uniformity of gas temperature in the combustion chamber.

Further, there is no noticeable difference in the range of post-injection timings where partial oxidation reactions occur based on post-injection quantity, indicating that fuel spray over-mixing is not the primary cause of partial oxidation.

Under conditions where partial oxidation occurs, the CO emissions concentration increases, however no clear differences are observed based on post-injection quantity. When the post-injection quantity is reduced from 5.0 mm^3/cycle to 2.5 mm^3/cycle, the THC emissions concentration corresponds to this reduction and is generally about half of the previous value. The increase in CO and THC emissions concentrations compared to post injection after diesel combustion as shown in Figure 5, is due to these chemical species generated by HCCI combustion being emitted without further re-oxidation.

Based on these results, it is suggested that making the main combustion more premixed in diesel combustion, could be an effective way to exhaust post-injection fuel as HC emissions without partial oxidation.

Partial oxidation behavior of post-injection fuel when varying inhomogeneity in cylinder (Test 3)

The study evaluated the influence of actively changing the in homogeneity of temperature and equivalence ratio within the cylinder by after-injection of diesel fuel (direct injection) after n-hexane HCCI combustion. The aim is to assess the impact of mixture inhomogeneity in cylinder on the partial oxidation behavior of post-injection fuel.

Engine test conditions

The conditions of this experiments are presented in Table 6. After creating a homogeneous temperature and equivalence ratio distributions within the cylinder by the HCCI combustion of the pre-mixed mixture of n-hexane and air, a small amount of after-injection is performed to alter the distributions of heterogeneous equivalence ratio and non-uniform gas temperature in the cylinder. The post-injection timing was varied in 11 steps within the range of 25 °CA ATDC to 60 °CA ATDC. The equivalence ratio of n-hexane was adjusted to maintain an in-cylinder average oxygen concentration of 16.0% during post injection. The fuel quantity of "after injection" was set at 1.0, 2.0, and 3.0 mm^3/cycle in three steps to vary the heterogeneity of equivalence ratio and the non-uniformity of gas temperature in the post injected circumstance in the cylinder while conducting single stage post injection at 5.0 mm^3/cycle.

Test results and discussions in Test 3

In Figure 9, the emissions concentrations of THC and CO at various post-injection timings are shown, and Figure 10 presents the heat release ratio of post-injection fuel. The heat release data of post-injection fuel are listed in Figure AP-3 in Appendix.

In Test 3, the different amount of after-injection fuel, 1-3mm^3/cycle of diesel fuel by direct injection at 10 °CA ATDC, are injected after the HCCI combustion. As the n-hexane quantity was adjusted to maintain the in-cylinder average oxygen concentration of 16.0% when the post-injection fuel is injected, the average temperatures inside the cylinder at the start of post-injection is the same, if the post-injection timings are the same. When comparing Figure 10 to post injection into a homogeneous environment as shown in Figure 8, fuel undergoes partial oxidation over a wide range of post-injection timing, resembling the partial oxidation behavior observed when post injection was carried out after diesel combustion as shown in Figure 6.

Further, for the conditions with after-injection quantities of 1.0 mm^3/cycle and 3.0 mm^3/cycle, there is approximately a 5 °CA difference in the post-injection timings where partial oxidation occurs. Though the atmosphere at the start of post injection becomes more heterogeneous with increasing after-injection quantity, the decreasing trend in the proportion of heat release of post-injection fuel when delaying the post-injection timing (θ_{post}) is consistent regardless of the after-injection quantity.

The experimental results in Tests 1-3 suggest that the partial oxidation of post-injection fuel is considered to be highly sensitive to the heterogeneity of equivalence ratio and the non-uniformity of gas temperature, however we cannot conclude which effect is more significant. Therefore, a three-dimensional CFD simulation analysis was conducted to investigate the partial oxidation phenomena from the points of heterogeneity of equivalence ratio and the non-uniformity of gas temperature in the next chapter.

Investigation of partial oxidation mechanism of single-stage post-injection fuel by three-dimensional CFD analysis

Three-dimensional CFD analysis (3D-CFD) was conducted on the partial oxidation behavior of post-injection fuel. The analysis aimed to examine the influence of the heterogeneity in temperature and equivalence ratio of the post-injection atmosphere on the partial oxidation behavior of single state post-injection fuel. Factors and mechanisms of partial oxidation reactions were analyzed and discussed.

Initial set-up of three dimensional CFD analysis

Computational conditions

The operating conditions under consideration correspond to Test 3 in Table 6, with an after-injection quantity of 1.0 mm^3/cycle. The computational conditions are presented in Table 7. In this analysis, calculations for HCCI combustion were not performed, however initial conditions were determined by the engine experimental data of HCCI combustion. To reproduce the heat release rate of after-combustion in actual experiments, the after-injection timing was set at 2 °CA lead and 8 °CA ATDC. Further, to quantitatively assess the partial oxidation of post-injection fuel, the mass and temperature of 12 chemical species handled by the ECFM-3Z model were extracted for all cells. The mass distributions of fuel (n-Heptane) and CO in each temperature range were then calculated.

Demonstration of calculation accuracy

Figure 11 presents the calculation results of the cylinder average pressure and heat release rate diagrams at the post-injection timing (θ_{post}) of 25 °CA ATDC, along with the corresponding experimental results under the same conditions. The calculated results successfully reproduce the heat release rate and combustion duration of the experimental results, and the parameters of the ECFM-3Z model fitted to this condition were applied to other post-injection conditions. Figure 12 compares the calculated results of the apparent heat release proportion of post-injection fuel with the experimental results. In the calculations, as in the experimental results, there is an inflection point during the decrease in heat release, qualitatively reproducing the decreasing trend in the heat release proportion due to partial oxidation associated with delaying the post-injection timing (θ_{post}).

Test results and discussions of three dimensional CFD analysis

Transitions of equivalence ratio, temperature and carbon monoxide distributions

Figure 13 illustrates the progress of the equivalence ratio distribution of the mixture formed by post-injection fuel. Here, the analysis is conducted under conditions where the post-injection timing (θ_{post}) is set at 25 °CA ATDC for complete combustion, 47.5 °CA ATDC and 52.5 °CA ATDC for partial oxidation, and 60 °CA ATDC for unburned conditions. The vertical axis represents the crank angle elapsed from each fuel injection timing, and the left figure of each column shows the combustion chamber section, while the right figure shows the spray axis section.

Under the condition with θ_{post} at 25 °CA ATDC, some of the post-injection fuel enters the combustion chamber and the majority enters the squish area. However, it does not reach the cylinder wall, and as the mixture gradually dilutes throughout the cylinder with the piston descent, it shows that the post-injection fuel is consumed by combustion. For conditions with θ_{post} of 47.5 °CA ATDC and later, all post-injection fuel impinges on the cylinder wall, and a relatively high equivalence ratio mixture remains near the cylinder wall.

For each condition, it can be observed that the post-injection fuel spray is influenced by swirl (given swirl ratio=2.23), flowing in the counterclockwise direction. The calculation using FIRE's sector model allows for the evaluation of the interaction between adjacent sprays by simulating the outflow of the mixture to the right of the diagram, which flows in from the opposite side. Even after the post-injection fuel spray reaches the cylinder wall, there is no confirmation of a high equivalence ratio region due to interference with adjacent sprays, and it suggests that the influence of swirl on mixture formation near the cylinder wall is small.

Figure 14 shows the transition of the temperature distribution (oxidation reaction region) of the mixture formed by post-injection fuel. Under the condition with θ_{post} at 25 °CA ATDC, at the 5 °CA point after the start of post injection, the entire post-injection fuel spray generates heat above 1500 K, indicating active combustion.

Under partial oxidation conditions with θ_{post} set at 47.5 °CA ATDC and 52.5 °CA ATDC, a rich region due to afterburning is formed near the fuel injection nozzle at the 5 °CA point after the start of post injection. From this high temperature region, heat release from post-injection fuel begins, and subsequent heating from the post-injection fuel that had reached near the cylinder wall is observed. As the equivalence ratio distribution shown in Figure 13, it is noted that some of the mixture formed by the post-injection fuel is flowed onto the lower surface of the cylinder head and the top surface of the piston after reaching the cylinder wall. As seen in Figure 15, under partial oxidation conditions with θ_{post} set at 47.5 °CA ATDC and 52.5 °CA ATDC, the post-injection fuel is partially oxidized near the cylinder wall progress, and CO is formed.

Under the condition with θ_{post} at 60 °CA ATDC, no heat release from post-injection fuel is observed in Figure 14. Under partial oxidation reaction conditions (θ_{post} =47.5 and 52.5 °CA ATDC) and unburned condition (θ_{post} =60 °CA ATDC), the difference in equivalence ratio distributions is small in Figure 13, however, in Figure 14, there is a significant difference in temperature heterogeneity. Based on the results, it is considered that temperature heterogeneity has a stronger influence on the partial oxidation of post-injection fuel compared to equivalence ratio heterogeneity in the post-injection atmosphere.

Figure 15 illustrates the transition of the CO concentration distribution of the mixture formed by post-injection fuel. Under the condition with θ_{post} at 25 °CA ATDC, at the 5 °CA point after the start of post injection, oxidation reactions occur across the entire post-injection fuel spray, leading to the production of CO in the corresponding region. Subsequently, it gradually dilutes throughout the cylinder with the descent of the piston, and CO undergoes re-oxidation. Under partial oxidation conditions with θ_{post} set at 47.5 °CA ATDC and 52.5 °CA ATDC, at the 5 °CA point after the start of post injection, post-injection fuel ignites from the high temperature region near the fuel injection nozzle formed by afterburning, and the generation of CO in that region is confirmed. The oxidation reactions progress near the cylinder wall as shown in Figure 15, and the CO concentration remains high. However, no decrease in concentration is observed with the descent of the piston. It suggests that the oxidation reaction of CO near the cylinder wall is suppressed, and it remains unoxidized, contributing to the significant increase in CO emissions observed in partial oxidation conditions in actual experiments.

Under the condition with θ_{post} at 60 °CA ATDC, although there is a slight generation of CO in the region where it interferes with the high temperature region formed by afterburning near the fuel injection nozzle, it gradually dilutes with the descent of the piston, and oxidation reactions leading to CO generation do not occur.

Quantitative evaluation of fuel and carbon monoxide distributions in cylinder

To quantitatively evaluate partial oxidation reactions, Figure 16 illustrates the mass distribution of fuel (n-Heptane) at 5, 10, 15, 20, and 25 °CA after the start of post injection.

Under the condition where the post-injection timing (θ_{post}) is set at 25 °CA ATDC, where all the fuel is combusted, at the 5 °CA point after the start of post injection, no fuel is present in temperature ranges below 1000 K, indicating rapid progress of oxidation reactions.

When delaying the post-injection timing beyond 47.5 °CA ATDC, it can be observed that in the temperature range of 400 K to 900 K, corresponding to the self-ignition temperature, fuel is present where oxidation reactions are not progressing. For instance, under the condition with θ_{post} set at 47.5 °CA ATDC, as the piston descends, the region of fuel presence shifts towards the lower temperature side, and the fuel mass decreases. This confirms partial oxidation of post-injection fuel.

Under the condition with θ_{post} set at 60 °CA ATDC, although the region of fuel presence shifts towards the lower temperature side as the piston descends, no decrease in fuel mass is observed, suggesting that oxidation reactions of the fuel are not progressing.

Figure 17 illustrates the mass distribution of carbon monoxide (CO) at 5, 10, 15, 20, and 25 °CA after the start of post injection. It should be noted that CO present in temperature ranges below 1000 K mainly results from simulating the initial composition resembling HCCI combustion and contributions from afterburning. Under the condition where the post-injection timing (θ_{post}) is set at 25 °CA ATDC, CO is generated in the temperature range of 1300 K to 2000 K at the 5 °CA point after the start of post injection and decreases with piston descent.

Under partial oxidation conditions with θ_{post} delayed to 47.5 °CA ATDC and 52.5 °CA ATDC, no CO generation is observed in temperature ranges above 1000 K at the 5 °CA point after the start of post injection, however the mass of CO increases with piston descent. This increase in CO production under such partial oxidation conditions qualitatively aligns with trends observed in the experiments, suggesting the possibility of CO generation above 1000 K.

Under the condition where θ_{post} is set at 60 °CA ATDC, the CO production at 5 °CA after the start of post-injection is lower compared to other conditions, and no significant mass change is observed with piston descent. This is attributed to the fact, as shown in Figure 15, that oxidation reactions of the fuel do not lead to CO generation in this condition.

Conclusions

In this study, both experimental tests with variations in the temperature and equivalence ratio heterogeneity of the post-injection ambient conditions and three-dimensional Computational Fluid Dynamics (3D-CFD) analyses were conducted to extensively analyze the factors and mechanisms behind the partial oxidation reactions of post-injection fuel.

The ignition and oxidation characteristics of the single stage post-injection fuel were analyzed, and the obtained results are summarized as follows:

1. The primary factors influencing the partial oxidation phenomenon of post-injection fuel are the heterogeneity of equivalence ratio and the non-uniformity of gas temperature in the post-injection ambient conditions and the results of the three-dimensional CFD analysis indicate that the non-uniformity of gas temperature has a stronger impact on partial oxidation of post-injection fuel than the heterogeneity of equivalence ratio.
2. In early post injection, since the cylinder is at a high temperature-pressure conditions, all post-injection fuel combusts before reaching the cylinder wall, making it impossible to supply hydrocarbons effective for diesel oxidation catalysts to re-generate the diesel particulate filters.
3. Under partial oxidation conditions, post-injection fuel initiates heat generation from the high temperature regions in the cylinder, and oxidation reactions mainly progress near the cylinder wall.
4. After post-injection fuel reaches the cylinder wall, the fuel not involved in oxidation reactions and transported towards the cylinder head underside and piston head direction is exhausted as unburned hydrocarbons. Additionally, a significant amount of CO, remaining without re-oxidation near the cylinder wall, is exhausted.
5. The partial oxidation of post-injection fuel with a delayed post-injection timing is attributed to the freezing of the oxidation reactions of fuel in the low temperature range

(400 K to 900 K), which is below the self-ignition temperature, due to piston descent and quench.

Acknowledgement

This paper is obtained as a result of a grant project (JPNP21014) conducted by The Research association of Automotive Internal Combustion Engines (AICE) with support from the New Energy and Industrial Technology Development Organization (NEDO).

References

[1] Serrano, J. & Piqueras, P. & De la Morena, Joaquin & Sanchis, Enrique. (2019), "Late Fuel Post-injection Influence on the Dynamics and Efficiency of Wall-Flow Particulate Filters Regeneration" Applied Sciences.

[2] Yamamoto, K., Takeda, K., Kusaka, J., Kanno, Y., and Nagata, M., "Influence of Diesel Post-injection Timing on HC Emissions and Catalytic Oxidation Performance", SAE Technical Paper 2006-01-3442, 2006

[3] Bobba., M., Musculus, M., and Neel, W., "Effect of Post Injectios on In-Cylinder and Exhaust Soot for Low-Temperature Combustion in a Heavy-Duty Diesel Engine", SAE International Journal of Engines 2010-04-12, 3(1), 496-516, 2010

[4] O'Connor, J., and Musculus, M., "Post-injections for Soot Reduction in Diesel Engines: A review of Current Understanding", SAE International Journal of Engines V112-3, 2013-01-0917, 2013

[5] Jeftic, M., Asad, U., Han, X., Xie, K., Yu, S., Wang, M., and Zheng, M., "An Analysis of the Production of Hydrogen and Hydrocarbon Species by Diesel Post Injection Combustion", ASME 2011 Internal Combustion Engine Division Fall Technical Conference, ICEF2011-60135, pp 679-687, February 2012

[6] Martin, J., Sun, C., Boehman, A., and O'Connor J., "Experimental Study of Post-injection Scheduling for Soot Reduction in a Light -Duty Turbodiesel Engines", SAE Technical Paper 2016-01-0726, 2016

[7] Yan Wu, Pan Wang, Sheikh Muhammad Farhan, Jing Yi, and Lili Lei, "Effects of post-injection on combustion and exhaust emissions in diesel engine", Fuel Volume 258, 116131, 2019

[8] Kojima, K., Kawanabe, H., and Kitamura, T., "Prediction of Oil Dilution by Post-injection in DPF Regeneration Model (First Report) Prediction of Fuel Adhesion Amount Based on 1-D Spray Development Model", Transactions of Society of Automotive Engineers of Japan, Vol. 50(5), 1230-1235, 2019

[9] Kojima, H., and Kawanabe, H., and Kitamura, T., "Prediction of Oil Dilution by Post-injection in DPF Regeneration Mode (1st Report)", JSAE Research Paper 20194667, pp

1230-1235, 2019 September

[10] Ito, T., Kitamura, T., Kojima, H., and Kawanabe, H., “Prediction of Oil Dilution by Post-injection in DPF Regeneration Mode (2nd Report), Prediction of Fuel Evaporation from Diluted Oil”, JSAE Research Paper 20194668, pp 1236-1241, 2019 September

[11] Ito, T., Kitamura, T., Kojima, H., and Kawanabe, H., “Prediction of Oil Dilution by Post-injection in DPF Regeneration Mode”, SAE Technical Paper 2019-01-2354, 2019

[12] Ito, T., Kitamura, T., Kojima, K., and Kawanabe, H., “Prediction of Oil Dilution by Post-injection in DPF Regeneration Model (Second Report) Prediction of Fuel Evaporation from Diluted Oil”, Transactions of Society of Automotive Engineers of Japan, Vol. 50(5), 1236-1241, 2019

[13] Matsuoka, M., Ito, T., and Kitamura, T., “Analysis of Oil Dilution Mechanism due to Post-injection for Diesel Particulate Filter (DPF) Regeneration” JSAE Transaction Paper Vol 47, No.6 pp 1317-1322, 2016 November

[14] Budde, M., Ehrly, M., Jakob, M., Wittler M., and Pischinger, S., “Simulation and optical analysis of oil dilution in diesel regeneration operaton”, SAE Technical paper 2011-01-1844, 2011

[15] Shibata, G., Nishiuchi, S., Puqing, X., Takai, S., Ogawa, H., and Kobashi, Y., “Measurements of fuel adhesion on cylinder walls and fuel wall-flow behavior with post diesel fuel injections”, International Journal of Engine Research, 2020, vol. 21(2) 352-366, 2020

[16] Shibata, G., Nishiuchi, S., Takai, S., Kobashi, Y., Kanbe, H., and Matsumura, E., “Fuel adhesion and oil splash on oil-wet cylinder walls with post diesel fuel injections”, International Journal of Engine Research, 2021, vol. 22(5) 1685-1701, 2021

[17] Shibata, G., Li, Y., Karumai, K., Kobashi, Y., and Ogawa, H., “Oxidation phenomena of diesel post fuel in the expansion stroke”, International Journal of engine Research, 2022, vol.24(3), 1095-1109

[18] Beale, J. C. and Reitz, R. D., “Modeling Spray Atomization with the Kelvin-Helmholtz/Rayleight-Taylor Hybrid Model”, Atomization and Sprays, Vol. 9, pp 623-650, 1999

[19] Dukowicz, J. K., “Quasi-stedy Droplet Change in the Presence of Convection”, Informal Report Los Alamos Scientific Laboratory, LA7997-MS, 1979

[20] Han, Z., and Reitz, R. D., “A Tempearature Wall Function Formulation for Variable Density Turbulent Flows with Application to Engine Convective Heat Transfer Modeling”, International Journal of Heat and Mass Transfer, 40, pp 6113-625, 1997

[21] Hanjalic, K., Popovac , M. and Hadziabdic, M.,“A Robust Near-Wall Elliptic-Relaxation Eddy-Viscosity Turbulence Model for CFD”, International Journal of Heat and Fluid Flow,

Vol.25, pp.1047-1051 (2004)
[22] Popovac, M. and Hanjalic, K.,"Compound Wall Treatment for RANS Computation of Complex Turbulent Flows and Heat Transfer", Flow, Turbulence, and Combustion, Vol.78, pp.177-202 (2007)
[23] Molina, S., Desantes, J., Garcia, A., and Postor, J., "A Numerical Investigation on Combustion Characteristics with the use of Post-injection in DI Diesel Engines", SAE Technical Paper 2010-01-1260, 2010

Appendix

The heat release data in Tests 1-3 are shown in Figure AP-1, AP-2, and AP-3.

Table 1 Specifications of test engine

Bore and stroke	ϕ86 × 86 mm
Displacement	1998 cm^3
Compression ratio	15.8
Swirl ratio	2.23
Combustion chamber	Re-entrant
Fuel injection system	Diesel : Common rail system
	HCCI : Intake pipe injection
Nozzle specification	ϕ0.09 mm × 9 - 155°
Air-charging system	Heated, Turbocharged

Table 2 Properties of test fuel

Property	JIS No.2 Diesel
Average number of carbons	16.357
Average number of hydrogens	30.491
Density [g/cm^3]	0.8214 (@15°C)
Kinematic viscosity [cSt]	3.034 (@30°C)
Lower heating value [MJ/kg]	42.91
10% Distillation temp. [°C]	189.5
50% Distillation temp. [°C]	266.5
90% Distillation temp. [°C]	338.5

Table 3 Sub-models in CFD code AVL FIRE

Turbulence	k-ζ-f
Spray	Discrete droplet model
Breakup	KH-RT
Evaporation	Dukowicz
Heat transfer	Han-Reitz
Combustion	Coherent Flame Model (ECFM-3Z)

Table 4 Test conditions of conventional diesel post injection (Test 1)

Engine speed [rpm]	1200
Intake gas pressure [kPa]	110
Intake gas temperature [°C]	100
Intake O_2 concentration [vol.%]	21
Diesel injection pressure [MPa]	50
Pilot injection timing [°CA ATDC]	-7.9
Pilot injection quantity [mm^3/cycle]	1.5
Pre injection timing [°CA ATDC]	-6.2
Pre injection quantity [mm^3/cycle]	2.1
Main injection timing [°CA ATDC]	-1.3
Main injection quantity [mm^3/cycle]	8.4
Post injection timing, θ_{post} [°CA ATDC]	25, 30, 35, 40, 42.5, 45, 47.5, 50, 52.5, 55, 60
Post injection quantity [mm^3/cycle]	5.0
In-cylinder O_2 concentration at post injection timing [vol.%]	16.0
IMEP of main combustion [MPa]	0.2

Table 5 Test conditions of post fuel injection in HCCI circumstances (Test 2)

Engine speed [rpm]	1200
Intake gas pressure [kPa]	110
Intake gas temperature [°C]	100
Intake O_2 concentration [vol.%]	21
Diesel injection pressure [MPa]	50
Post injection timing, θ_{post} [°CA ATDC]	25, 30, 31, 32, 33, 34, 35, 40
Post injection quantity [mm^3/cycle]	2.5, 5.0
In-cylinder O_2 concentration at post injection timing [vol.%]	16.0
Equivalence ratio of n-Hexane [-]	0.26
IMEP of HCCI combustion [MPa]	0.25

Table 6 Test conditions of post fuel injection in heterogeneous circumstances (Test 3)

Engine speed [rpm]	1200
Intake gas pressure [kPa]	110
Intake gas temperature [°C]	100
Intake O_2 concentration [vol.%]	21
Diesel injection pressure [MPa]	50
After injection timing [°CA ATDC]	10
After injection quantity [mm^3/cycle]	1.0, 2.0, 3.0
Post injection timing, θ_{post} [°CA ATDC]	25, 30, 35, 40, 42.5, 45, 47.5, 50, 52.5, 55, 60
Post injection quantity [mm^3/cycle]	5.0
In-cylinder O_2 concentration at end of HCCI combustion [vol.%]	16.0
Equivalence ratio of n-Hexane [-]	0.26
IMEP of HCCI combustion [MPa]	0.25

Table 7 3D-CFD calculation conditions

Calculation range [°CA ATDC]]	-20 - 120
Calculation time step [°CA]	0.1
Initial temperature [K]	1180
Initial pressure [MPa]	3.4
After injection timing [°CA ATDC]	8
After injection quantity [mm^3/cycle]	1.0
Post injection timing, θ_{post} [°CA ATDC]	25, 30, 35, 40, 42.5, 45, 47.5, 50, 52.5, 55, 60
Post injection quantity [mm^3/cycle]	5.0
Cylinder wall temperature [K]	450
Swirl ratio	2.23
Fuel	n-Heptane
Initial chemical species composition (mole fraction)	
O_2	0.16
H_2O	0.01
CO	0.0017
CO_2	0.04
N_2	0.7883
ECFM-3Z model parameter	
Spark ignition model	Not applicable
Mixing model parameter [-]	0.45
Auto ignition model	Two-stage
Auto ignition model parameter [-]	5.0
Chemical reaction time [s]	3.5
Extinction temperature [K]	1000

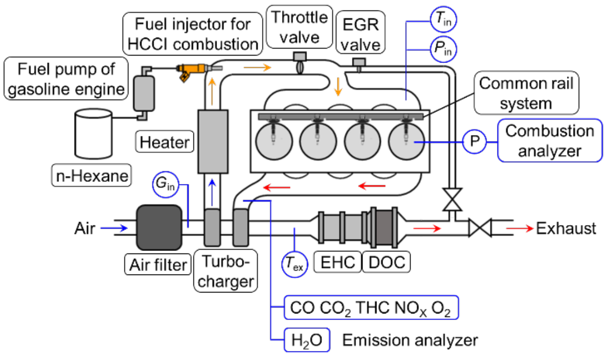

Fig. 1 Test engine set-up

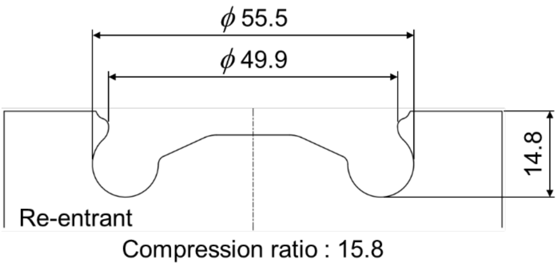

Fig. 2 Shape of re-entrant piston top

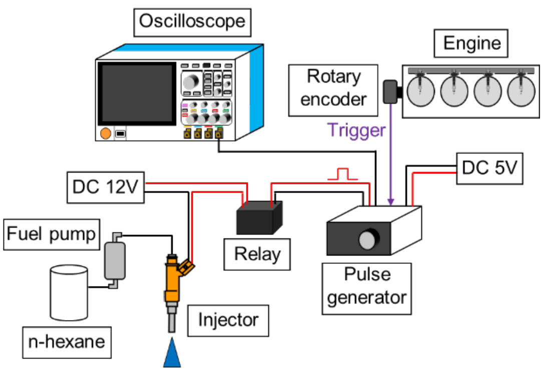

Fig. 3 Port fuel injection system for HCCI operation

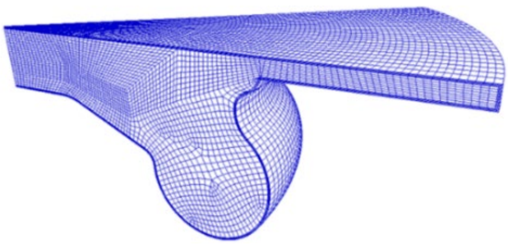

Fig. 4 Computational mesh for 3D-CFD

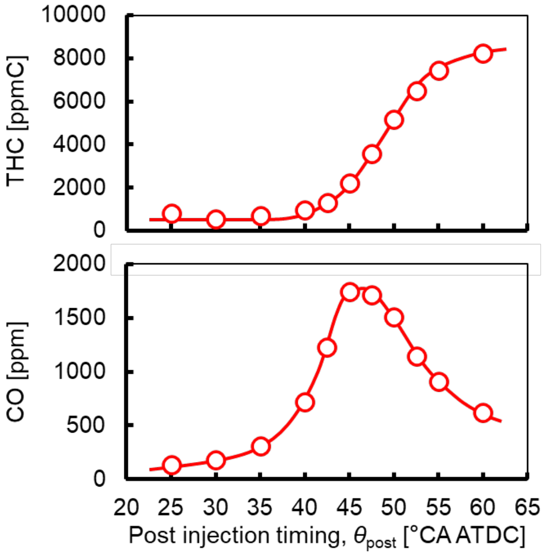

Fig. 5 Effects of post injection timing (θ_{post}) on CO and THC emissions (Test 1)

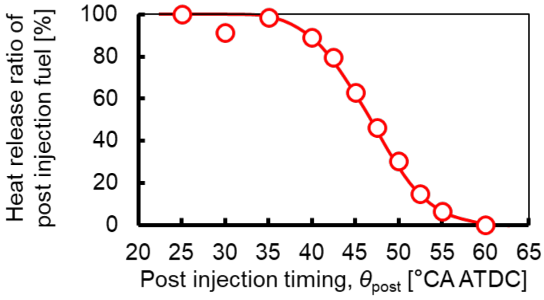

Fig. 6 Effects of post injection timing (θ_{post}) on heat release rate of post injection fuel (Test 1)

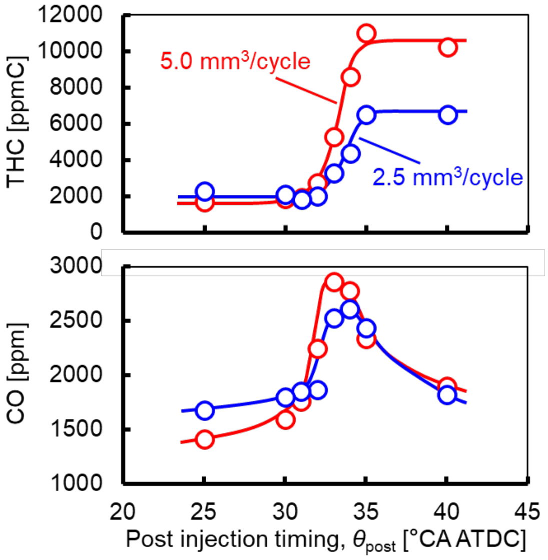

Fig.7 Effects of post injection timing (θ_{post}) on CO and THC emissions (Test 2)

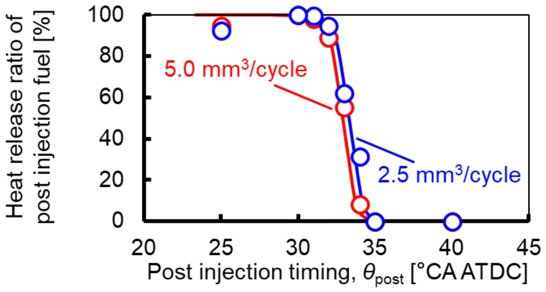

Fig. 8 Effects of post injection timing (θ_{post}) on heat release rate of post injection fuel (Test 2)

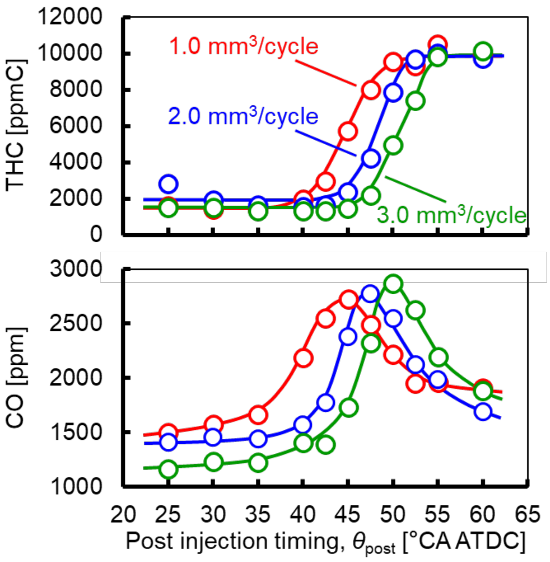

Fig. 9 Effects of post injection timing (θ_{post}) on CO and THC emissions (Test 3)

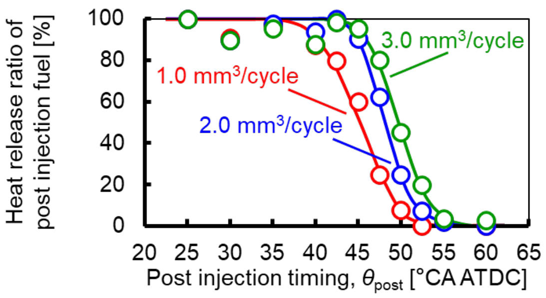

Fig. 10 Effects of post injection timing (θ_{post}) on heat release rate of post injection fuel (Test 3)

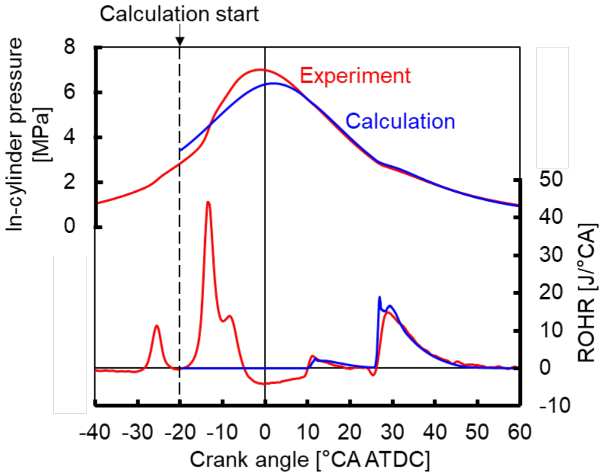

Fig. 11 Comparison of experiment and simulation data on in-cylinder pressure and rate of heat release

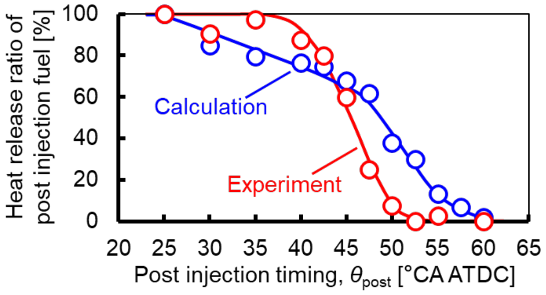

Fig. 12 Comparison of experiment and simulation data on heat release ratio of post injection fuel

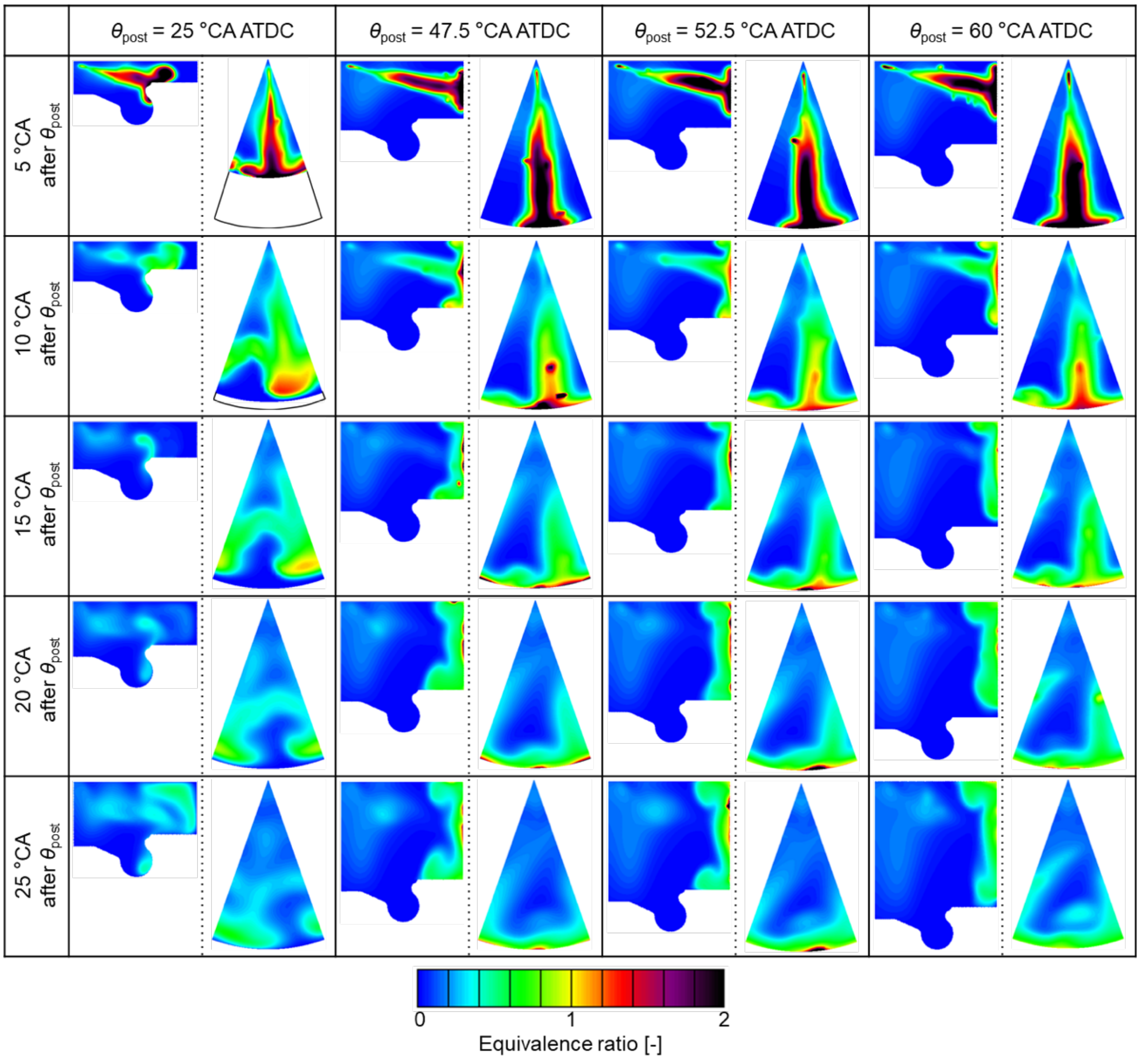

Fig. 13 Transition of equivalence ratio distribution after post injection

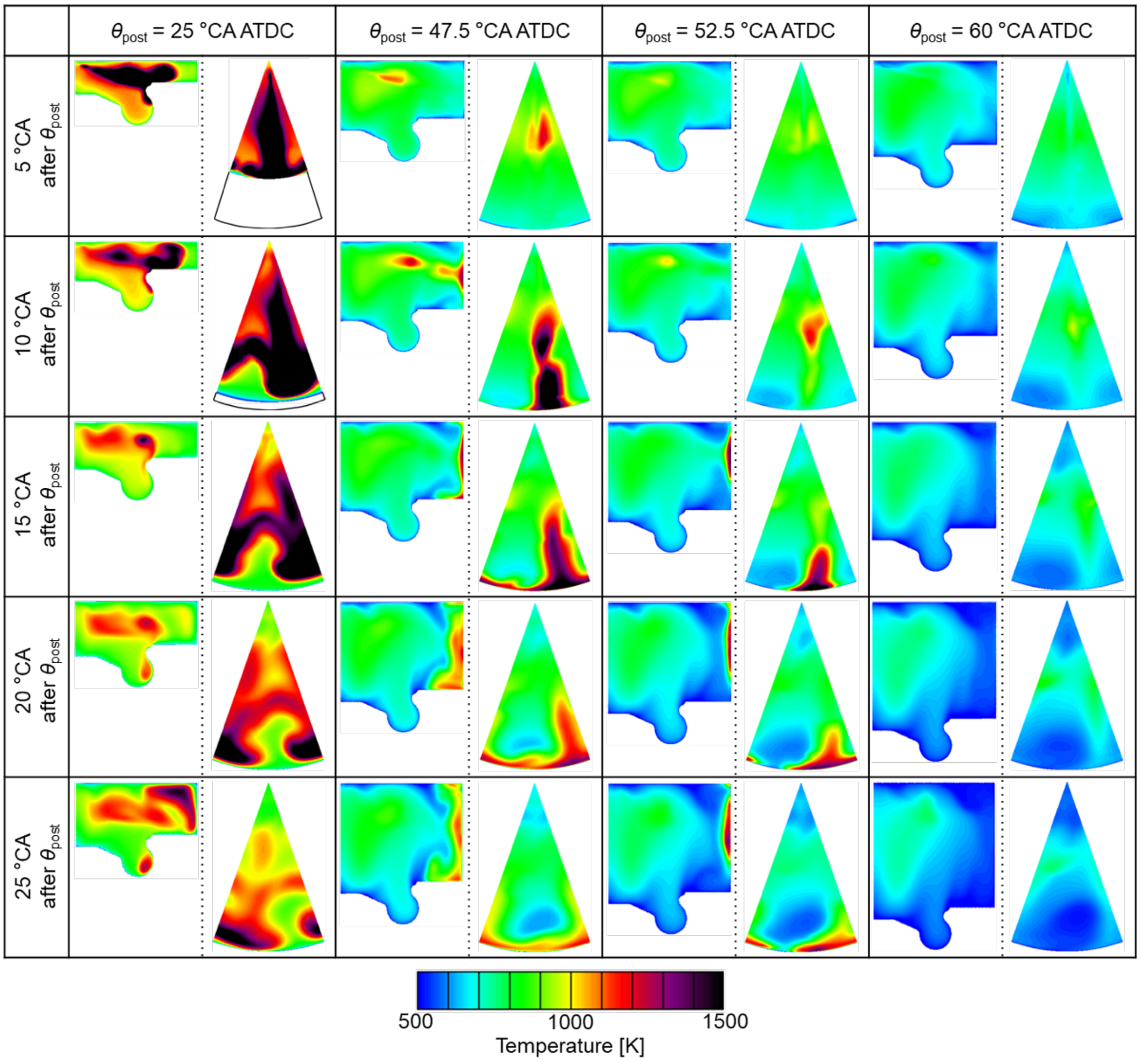

Fig. 14 Transition of temperature distribution after post injection

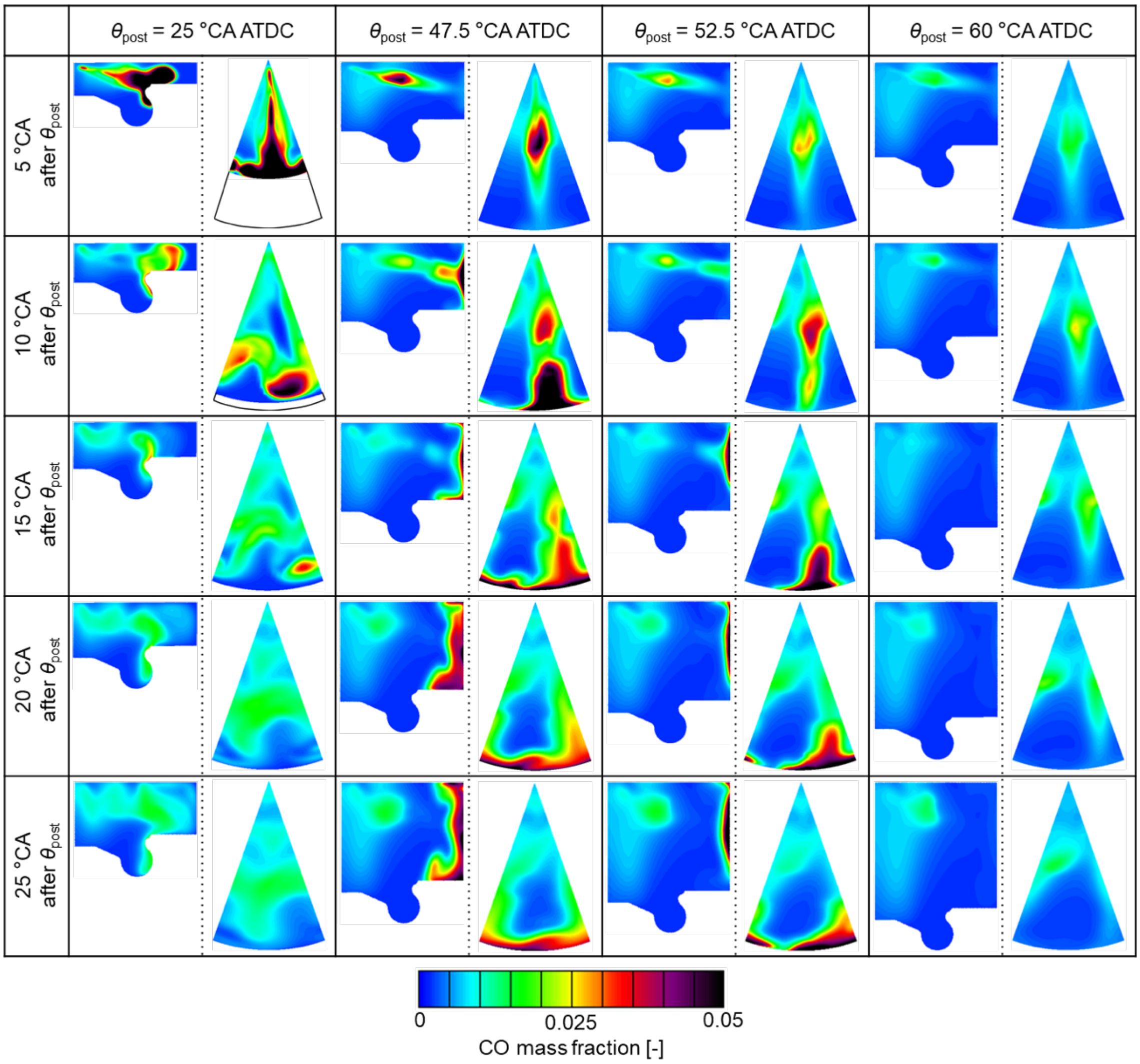

Fig. 15 Transition of carbon monoxide (CO) distribution after post injection

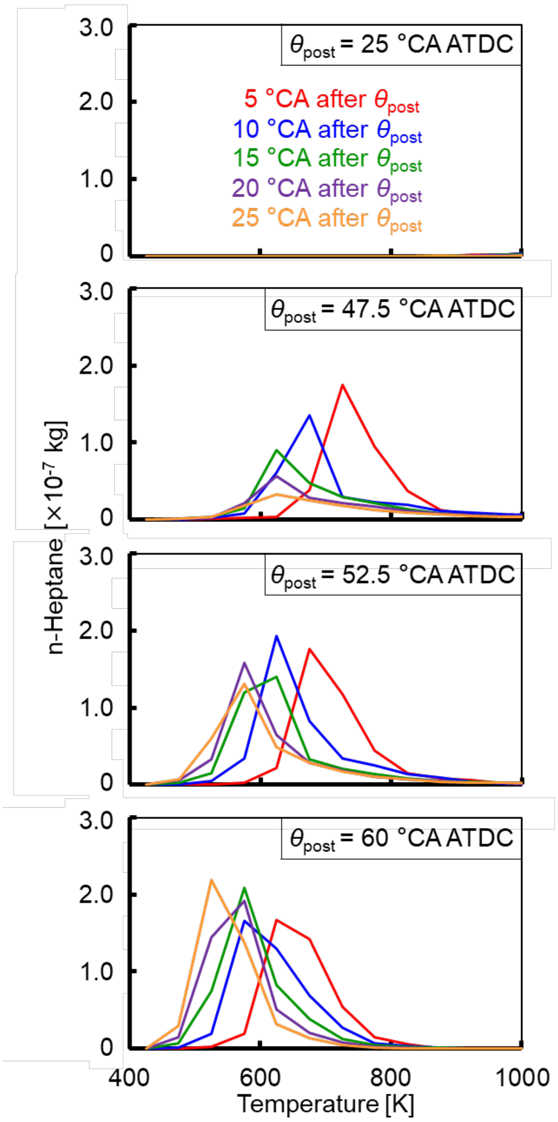

Fig. 16 Mass distribution of fuel (n-heptane) in each temperature range

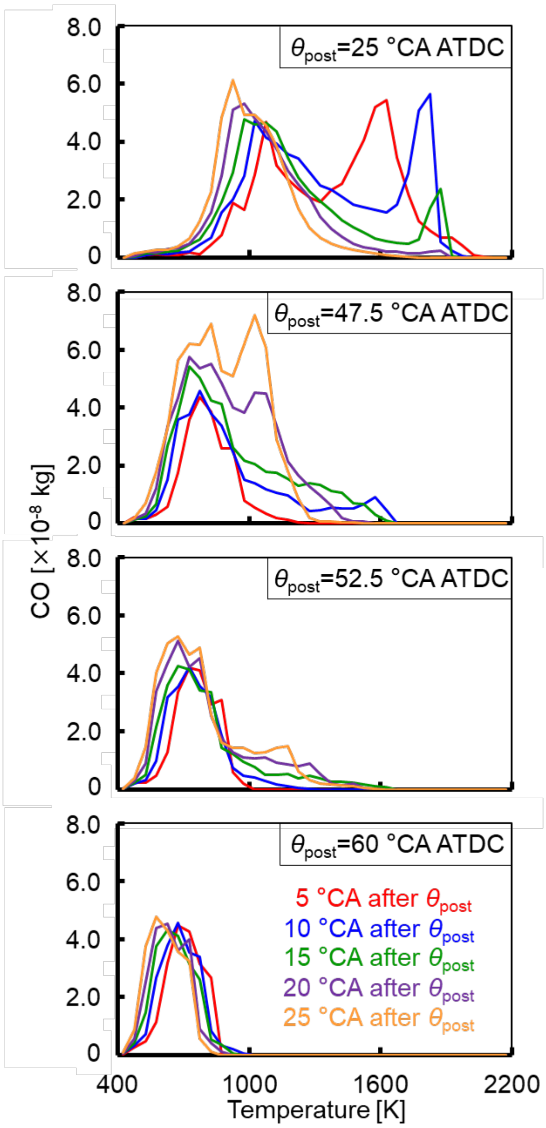

Fig. 17 Mass distribution of carbon monoxide (CO) in each temperature range

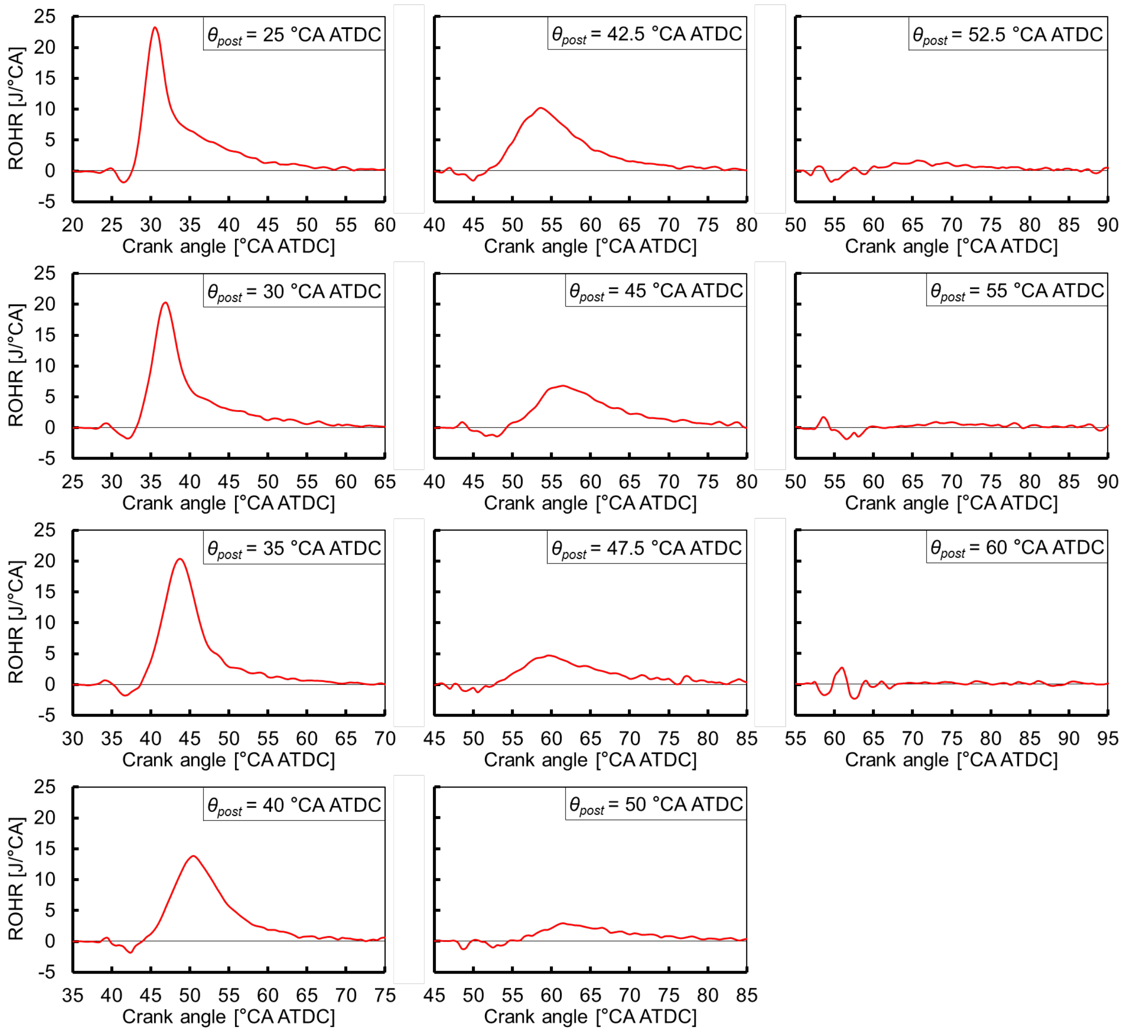

Fig. AP-1 Comparison of heat release rate when the post-injection timing is changed (Test 1)

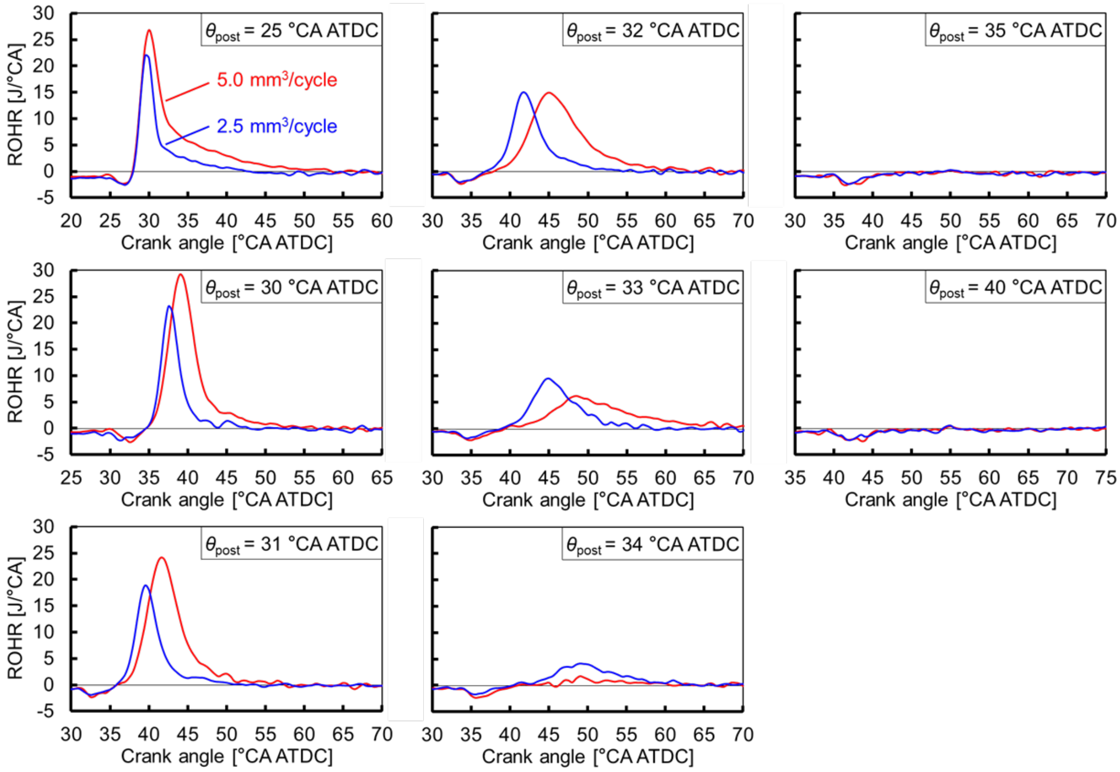

Fig. AP-2 Comparison of heat release rate when the post-injection timing is changed (Test 2)

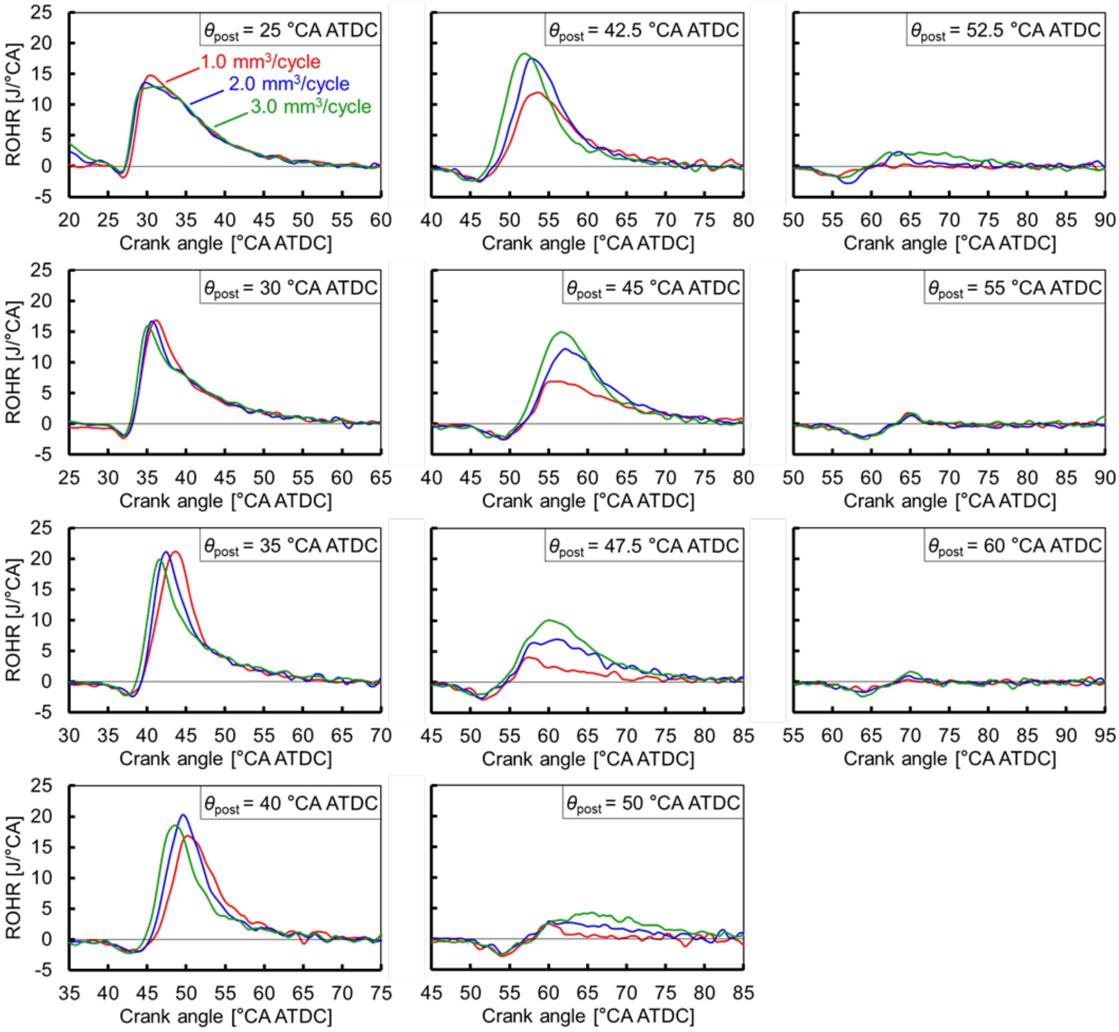

Fig. AP-3 Comparison of heat release rate when the post-injection timing is changed (Test 3)